



D4.4

Prototype of Fabricated and Characterized Sensor Interface

Project number:	644039
Project acronym:	M3TERA
Project title:	M3TERA – Micromachined terahertz systems – a new heterogeneous integration platform enabling the commercialization of the THz frequency spectrum
Start date of the project:	1 st February, 2015
Duration:	45 months
Programme:	H2020-ICT-2014-1

Deliverable type:	Demonstrator
Deliverable reference number:	ICT-644039 / D4.4 / V2.0
Work package contributing to the deliverable:	WP 4
Due date:	M41 – June 2018
Actual submission date:	7 th January, 2019

Responsible organisation:	KTH
Editor:	Joachim Oberhammer
Dissemination level:	Public
Revision:	V2.0

Abstract:	This document presents the characterisation of the multi-purpose THz sensor antenna interface, based on a micromachined waveguide interface.
Keywords:	Mm—wave antenna, IC interconnect, sensor, THz radar, THz applications



This project has received funding from the European Union's Horizon 2020 research and innovation programme under grant agreement No 644039.

This work is supported (also) by the Swiss State Secretariat for Education, Research and Innovation (SERI) under contract number 15.0059. The opinions expressed and arguments employed herein do not necessarily reflect the official views of the Swiss Government.

Editor

Joachim Oberhammer (KTH)

Contributors

Alexander Vorobyov, John Farserotu (CSEM)

Joachim Oberhammer (KTH)

Internal Reviewers (ordered according to beneficiary numbers)

Itziar Maestrojuan (Anteral)

Disclaimer

The information in this document is provided “as is”, and no guarantee or warranty is given that the information is fit for any particular purpose. The users thereof use the information at their sole risk and liability.

Executive Summary

D4.4 is a prototype deliverable about a micromachined sensor interface to be utilized in the sensor work of M3TERA, and comprising the sensor interface of the micromachined M3TERA platform. This report is a summary describing the prototype and summarizing the characterization results.

On the sensor and antenna side, D4.4 builds upon the results of D4.2 and D6.5, reporting on Concept and Design of Platform-Integrated Near-Field Interfaces for Secondary Prototype and Applications and Potential Utilization of the THz Microsystem Platform for Different High-Volume Sensor Applications.

On the micromachining side, D4.4 builds upon the technology development in D2.3, Micromachined Platform First Generation Prototype, and on the extraordinary work on the stand-alone telecommunication diplexers.

Thus, this prototype work is primarily a synergy result of the work packages WP2 and WP4.

Decisions on the antenna solutions presented in this report are based on D1.1, D6.1, where secondary applications were identified and specifically defined, and D4.2a, focusing on the mm-wave antenna solution for the M3TERA secondary application (sensing).

The focus of this deliverable is the characterization of low cost plastic 3D printed antennas integrated with the micromachined-waveguides in the M3TERA platform technology.

Contents

Chapter 1	Introduction	1
Chapter 2	Micromachined sensor interface	2
Chapter 3	Antennas prototyping and characterisation	6
3.1	Antenna prototyping.....	6
3.2	Measurement setup	7
3.3	Antenna radiation performance characterisation	8
Chapter 4	Summary and conclusion	10
Chapter 5	List of Abbreviations	11
Chapter 6	Bibliography	12

List of Figures

Figure 1:	Layout of micromachined-waveguide interface between dielectric radiating bodies and a standard waveguide flange.	2
Figure 2:	Fabricated chips before (left) and after (right) metallization.	3
Figure 3:	Assembled chips mounted on standard waveguide port adapters.	3
Figure 4:	Microscope picture of waveguide cross-section at open-ended waveguide tip. The waveguide size is 1651x825.5 mm ²	4
Figure 5:	Postbonding misalignment measurements.	5
Figure 6:	3D printer “REIFY 3D” for the antenna prototyping	6
Figure 7:	Prototyped plastic antennas.	6
Figure 8:	Antenna measurement setup.....	7
Figure 9:	Chip attachment to the WG section.	7
Figure 10:	Antennas under test.	8
Figure 11:	Micromachined waveguide radiation pattern measurement results.	8
Figure 12:	Rod antenna radiation pattern measurements at 122GHz.	9
Figure 13:	Flat 3D lens radiation pattern measurements.	9

List of Tables

Table 1:	Resin material EM properties.....	6
----------	-----------------------------------	---

Chapter 1 Introduction

At millimetre-wave frequencies, dielectric lens and dielectric rod antennas provide a significant performance vs cost advantage as compared to other high gain antennas such as horn antennas, which are often more expensive, bulky and difficult to manufacture.

3D printing, as utilized for this deliverable, makes such antenna solutions even more attractive, in particular from a cost and quick prototyping point of view. The surface properties of 3D-printed dielectric antennas are less critical than for metallized surfaces, and sufficient for frequencies below 200 GHz. 3D-printing allows in particular for fabricating complex 3D-shaped geometries, such as 3D elliptical hemispheres.

Chapter 2 Micromachined sensor interface

The micromachined-waveguide sensor interface comprises 4 parts:

- a standard waveguide flange (WR6.5, 1651 μm x 825.5 μm , 4 diagonal alignment pins) interface
- a wideband transition from vertical (1651 μm x 825.5 μm) to horizontal (1651 μm x 800 μm) micromachined waveguide
- a 20 mm long micromachined waveguide channel (1651 μm x 800 μm)
- a sharp waveguide tip, i.e. narrow waveguide walls in all dimensions around the waveguide opening

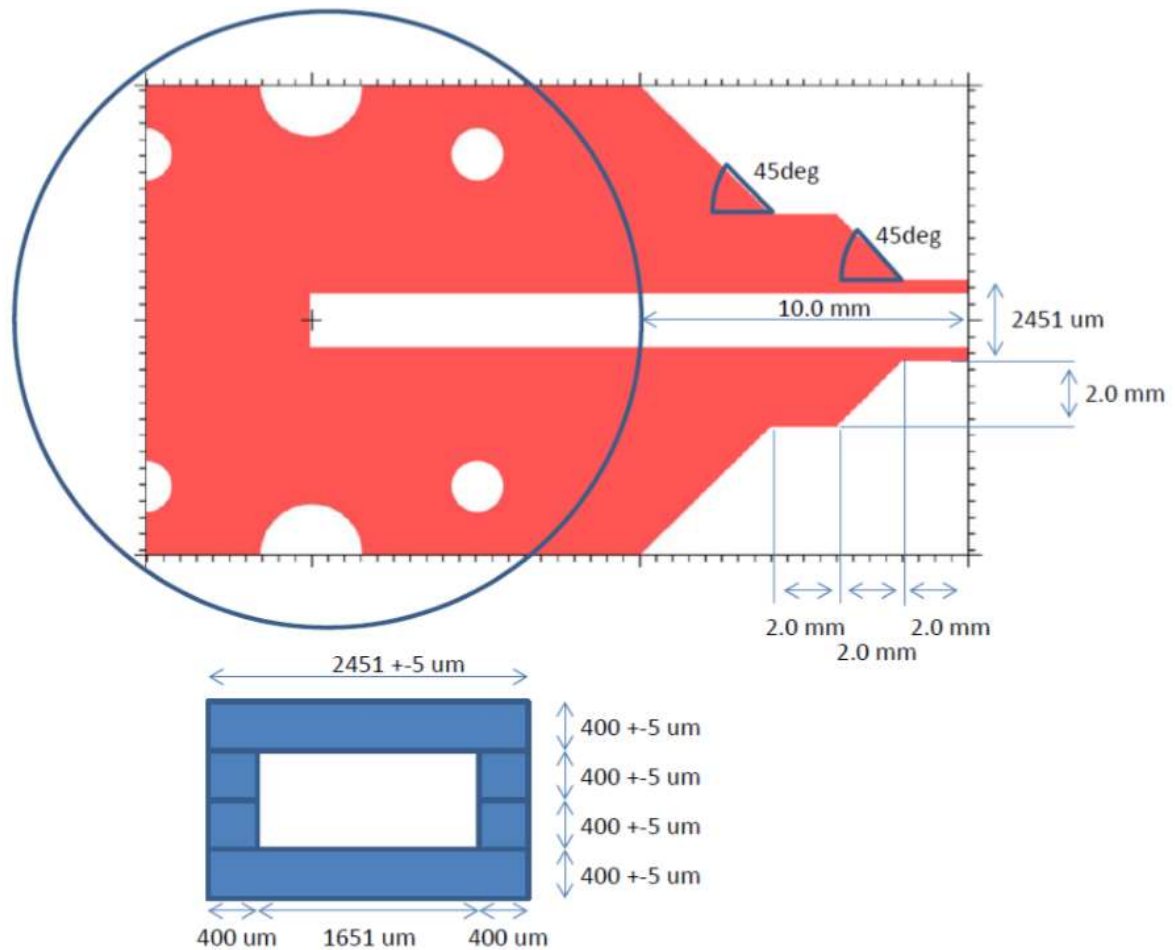


Figure 1: Layout of micromachined-waveguide interface between dielectric radiating bodies and a standard waveguide flange.

A top view of the micromachined chip is shown in Figure 1. The sharp waveguide tip is achieved by multiple tapers in order not to compromise the mechanical stability, and thus makes handling easy.

Figure 1 shows also the cross-section of the waveguide at the interface tip, showing the wall thicknesses in all 4 dimensions being 400 μm . It should be noted that the micromachined waveguide is slightly shallower than a standard waveguide, by 3.08%, which has a small but not a significant influence neither on the waveguide performance nor on the waveguide impedance.

The chip is composed of 4 wafers, all of which are etched with the following features:

- wafer 1 (top wafer): waveguide roof with opening in waveguide flange
- wafer 2 top part of micromachined waveguide, with vertical transission
- wafer 3 bottom part of micromachined waveguide, with vertical transission
- wafer 4 (bottom wafer): waveguide bottom

Alignment and screw holes are etched through all wafers.



Figure 2: Fabricated chips before (left) and after (right) metallization.

Figure 2 shows fabricated chips before assembly, before and after the metallization, and Figure 3 shows assembled 4-layer chips mounted on a standard waveguide port adapter.

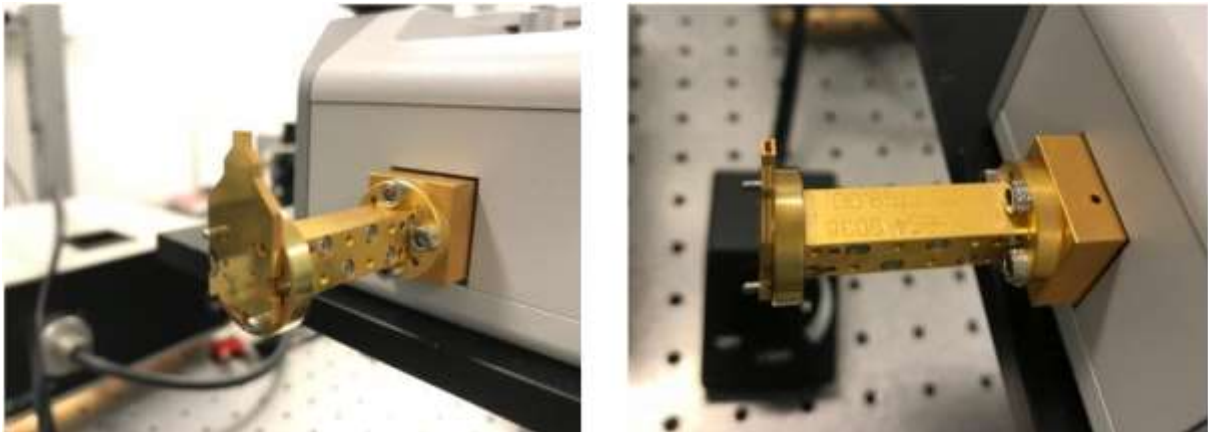


Figure 3: Assembled chips mounted on standard waveguide port adapters.

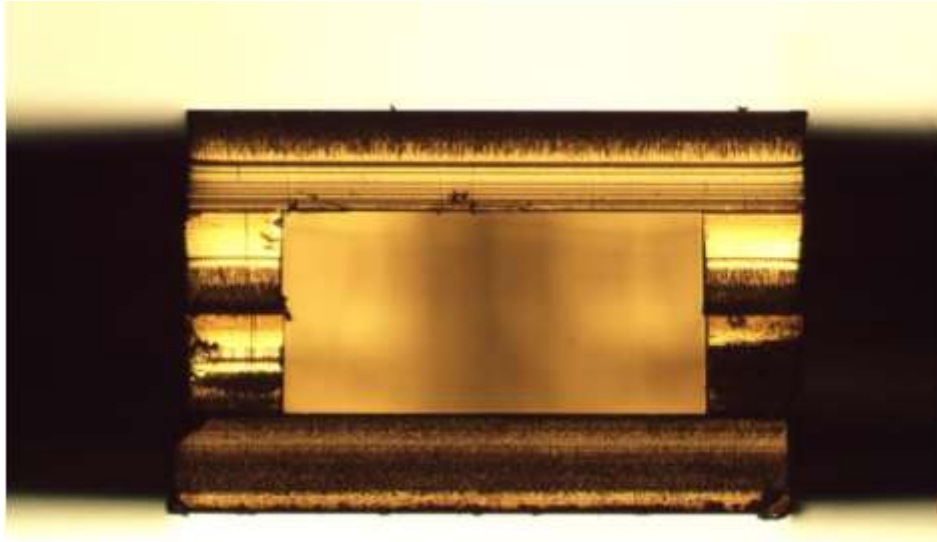
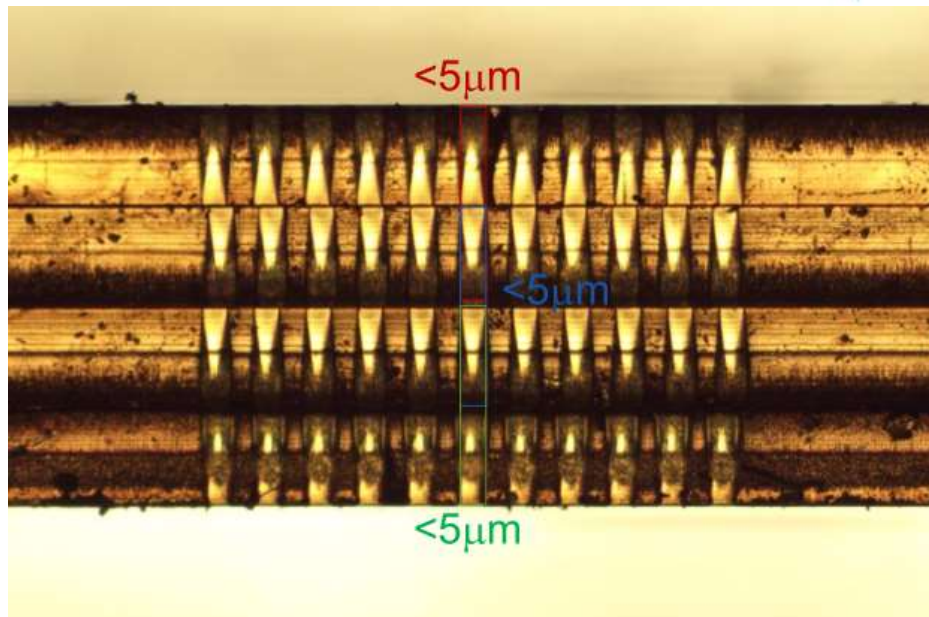
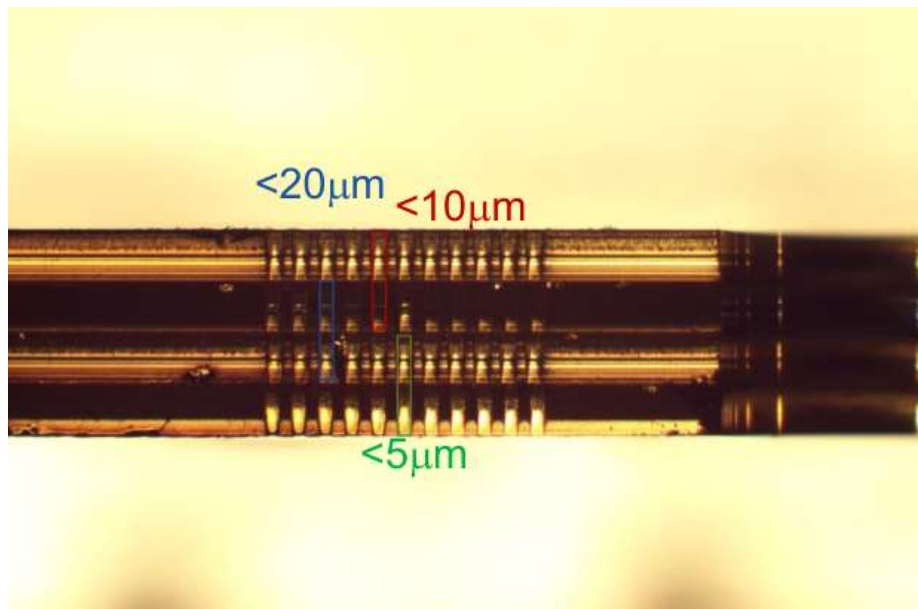


Figure 4: Microscope picture of waveguide cross-section at open-ended waveguide tip. The waveguide size is 1651x825.5 μm^2 .

Figure 4 shows the waveguide interface tip, on which the dielectric radiating bodies are to be mounted. The visible offset between the chips stems mainly from the underetching of the waveguides, which is in the order of 10 μm for the 400 μm tall chips.



(a) device with low post-bonding misalignment error in all 3 interfaces



(b) typical device with typical post-bonding misalignment errors

Figure 5: Postbonding misalignment measurements.

Figure 5 shows the measured post-bonding misalignment between the 4 chips for two different devices. For the device shown in subfigure (a), all 3 post-bonding misalignment errors were below $5\ \mu\text{m}$. For all chips fabricated, the worst-case post-bonding misalignment was found to be $30\ \mu\text{m}$, whereas average values of $10\ \mu\text{m}$ were typical for assembling these devices, as a simplified alignment procedure was used. A typical chip is shown in subfigure (b). Post-bonding misalignment of down to $2\ \mu\text{m}$ is possible at KTH, but requires a special alignment procedure which was not deemed necessary for these waveguide devices without any critical features.

Chapter 3 Antennas prototyping and characterisation

This chapter describes the prototyping and characterisation of the devices for the secondary sensing application, i.e. millimeter-wave antenna solutions interfacing the micromachined M3TERA platform. Three dielectric focusing antenna solutions are realised, and two of them have been assembled and characterised together with the micromachined platform based on the M3TERA technology.

3.1 Antenna prototyping

A REIFY 3D printer [1] has been used for fabricating the antennas prototyping. This is a stereolithography printer based on a DLP projector as presented in Figure 6. The antenna material is acrylate polymer, whose parameters are presented in Table 1.

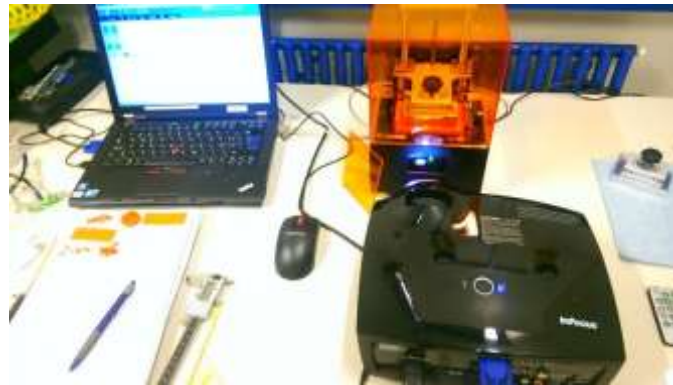


Figure 6: 3D printer “REIFY 3D” for the antenna prototyping

Acrylate polymer	
Relative permittivity (ϵ)	~ 3
Dielectric loss tangent ($\text{tg}\delta$)	6×10^{-4}

Table 1: Resin material EM properties

The antennas have been prototyped with better than 0.08 mm nominal accuracy. The shapes of the investigated antennas are shown in Figure 7.

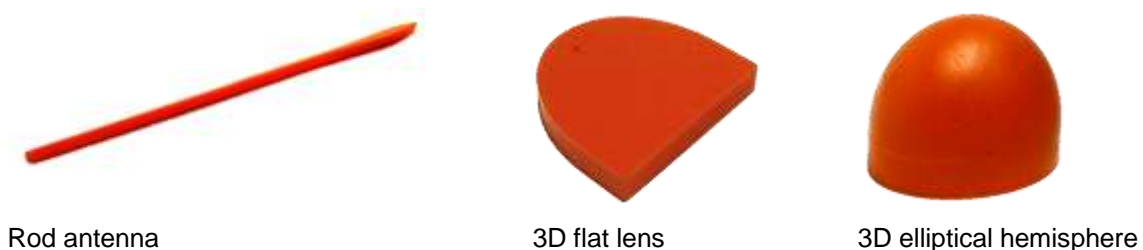


Figure 7: Prototyped plastic antennas.

3.2 Measurement setup

The antenna radiation characteristics were measured in the CSEM anechoic chamber. The antenna measurement setup is based on commercially available components and presented in Figure 8. The transmitter is equipped with a standard horn antenna operating in the ISM frequency band (121GHz-123GHz). The transmitter is connected to an external local oscillator (LO), which is also used for synchronizing the spectrum analyzer at the receiver side. The antenna under test (AUT) is mounted on a rotatable (360°) post mount with the possibility to measure both vertical and horizontal polarisation of the AUT. The measurement results are presented in section 3.3.

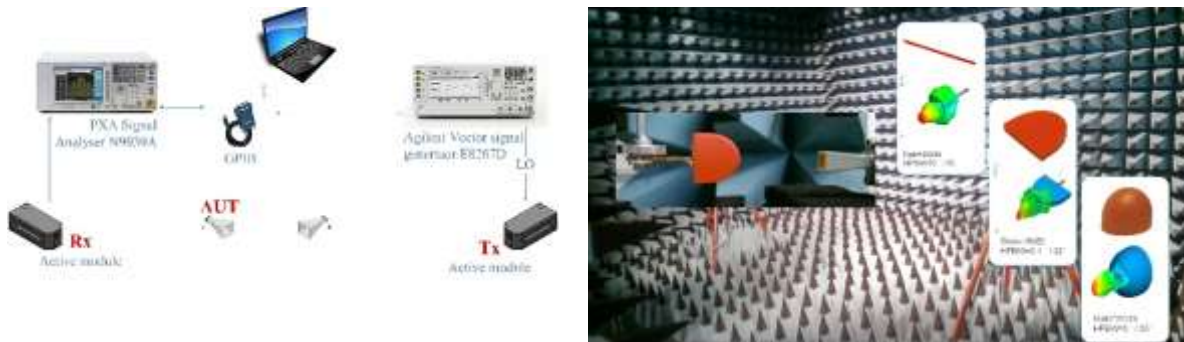


Figure 8: Antenna measurement setup

The micromachined waveguide (WG) section provided by KTH is connected to a standard WR-10 (UG-387) flange waveguide section as depicted in Figure 9. Two metallic bolts with plastic spacer rings have been used for fixating the micromachined WG section on the WG section. The plastic rings are used in order to protect the brittle silicone structure from damage.



(a) WG section with a chip

(b) chip attached to the WG section

(c) chip attached to the WG section and fixed

Figure 9: Chip attachment to the WG section.

Two antennas were characterised: 1) a rod antenna and 2) a flat 3D lens antenna. The rod antenna is directly inserted into the micromachined WG aperture. No further mechanical fixation is necessary. The lens antenna is attached to the WG with a small drop of plastic glue, as shown in Figure 10. This quick, relatively simple method allows for good fixation of the antenna and simplifies tear-off / replacement without damaging the WG micromachining.

The glue solution works well for small antennas, but relatively large (heavy) antennas glued to the chip can damage it. In this case, the lens should be mechanically fixated to the WG chip surrounding chassis and the lens antenna design should consider the influence of any mechanical fixture on the radiation.

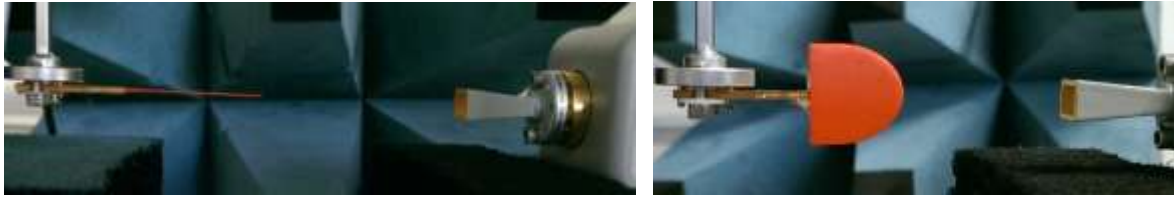


Figure 10: Antennas under test.

3.3 Antenna radiation performance characterisation

Three antennas have been characterized in the anechoic chamber.

These are:

- Micromachined open-ended waveguide;
- Dielectric focusing antenna solutions
 - o Rod antenna;
 - o Flat 3D antenna.

The antennas are optimized to operate in the mm-wave ISM band (122GHz-123GHz) and can be used in various RF sensing applications.

The measured radiation performance of the micromachined open waveguides is shown in Figure 11. The open-ended micromachined WG antenna gain and Half Power Beam Width (HPBW) are about 6dBi and 50 degrees respectively. The measured radiation pattern is very similar to the theoretically predicted, but the measured antenna gain is slightly less than the theoretically-predicted results (Figure 11). This can be explained by a possible misalignment of the micromachined chip and the WG section.

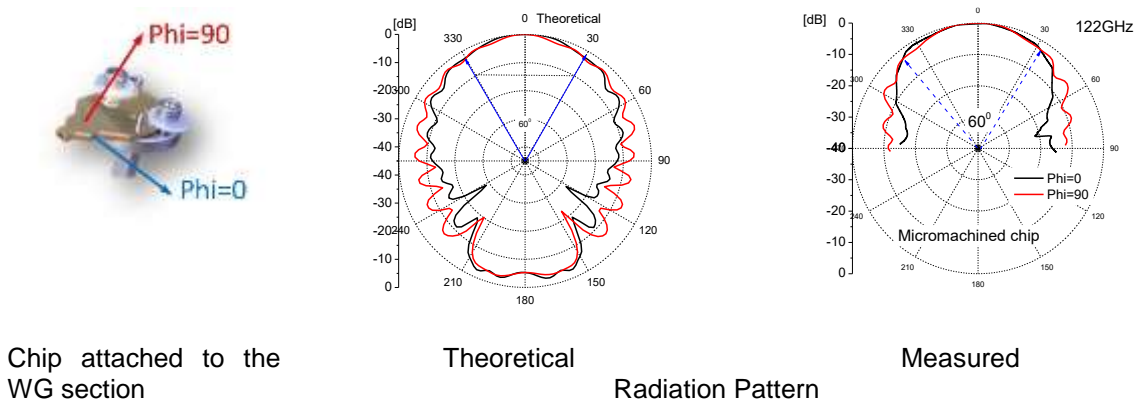
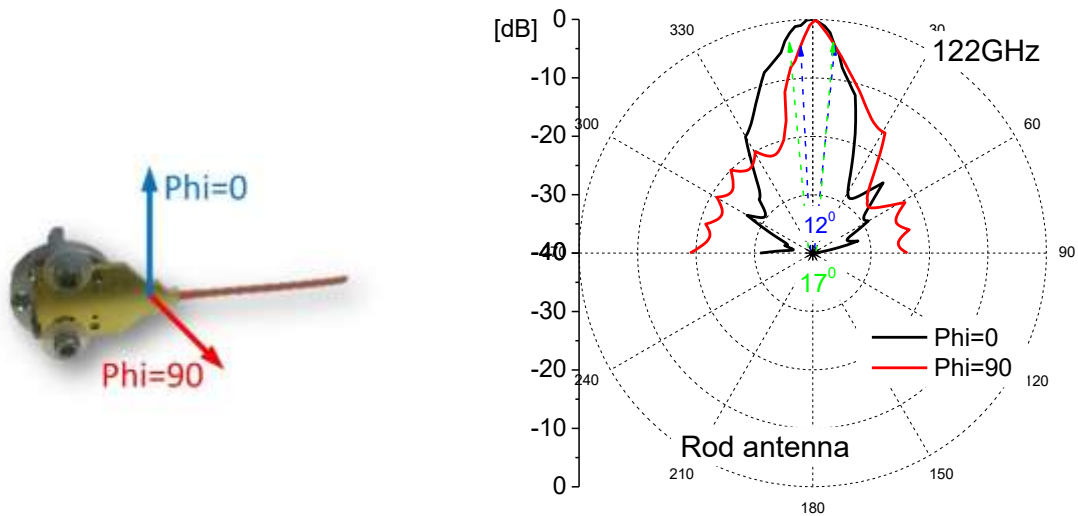


Figure 11: Micromachined waveguide radiation pattern measurement results.

The open-ended WG alone is a good candidate for the M3TERA secondary application where a large area of the object under test needs to be illuminated in specific user scenarios.

The dielectric-rod antenna measurement results are presented in Figure 12. The rod antenna gain and HPBW are about 16dBi and 17 degrees, respectively. The measured antenna radiation pattern is slightly asymmetrical. This can be explained by the nature of the antenna material. The material is soft, which can result in slight bending of the antenna during the test. This seems to be the case here, since the previously measured rod antenna (see D6.5, section 3.2) showed good symmetrical radiation pattern characteristics. To avoid such problems in the future, a more stable resin material with similar EM properties is suggested (e.g. FullCore 750).



Flat 3D lens antenna

Measured Radiation Pattern

Figure 12: Rod antenna radiation pattern measurements at 122GHz.

The antenna mounting inside the open WG section can also affect the antenna radiation pattern. In this case, additional alignment / fixation features can be included in the antenna design.

The results of the second prototype, a 3D flat lens antenna measurements are presented in Figure 13. The antenna gain was found to be about 17 dBi, with a HPBW of 6 and 13 degrees for the E and the H plane, respectively. The attachment of the radiation body posed a major difficulty with respect to the characterisation of this antenna due to the fragile WG section.



Flat 3D lens antenna

Measured Radiation Pattern

Figure 13: Flat 3D lens radiation pattern measurements.

Chapter 4 Summary and conclusion

Different low cost, plastic 3D-printed antenna solutions mounted on micromachined-waveguide interfaces have been fabricated and characterized: a flat lens, and a long rod. As a reference, an open-ended micromachined WG was characterized as well. The micromachined waveguide interface between the dielectric radiating bodies and a standard WR-6.5 waveguide flange were manufactured in a 4-layer microchip stack consisting of 400 μ m thick micromachined chips, resulting in a 1651 μ m x 800 μ m large waveguide cross-section. The antennas are optimized to operate at mm-wave ISM band (122GHz-123GHz) and demonstrated to work for various RF sensing applications. The techniques used can be easily extended to realize similar antennas operating at other mm-wave frequency bands. Using a 3D printer enabled us to rapidly prototype different plastic antennas that can be mechanically fitted to transmitting devices and thus modify the radiation performances.

The tested antennas demonstrated good overall radiation performance. The slight deviation in the antenna performance is explained by a possible misalignment attachment of the micromachined WG to the standard WG section, as well as the antenna mounting to the micromachined waveguide. The choice of a more suitable resin material would improve the antenna robustness and could additionally improve the antenna radiation performance.

Chapter 5 List of Abbreviations

PCB	Printed circuit board
LTCC	Low Temperature Co-Fired Ceramics
EM	Electro Magnetic
mmW	Millimetre wave
SIW	Substrate integrated waveguides
AUT	antenna under test
WG	waveguide
HPBW	half-power beam width
ISM	industrial, scientific, medical

Chapter 6 Bibliography

- [1] <http://www.reify-3d.com/products/>